Mineralogical Magazine (2023), **87**, 561–567
doi:10.1180/mgm.2023.30

CAMBRIDGE UNIVERSITY PRESS

Article

First occurrence of the *M2a2b2c* polytype of argentopolybasite, $[Ag_6Sb_2S_7][Ag_{10}S_4]$: Structural adjustments in the Cu-free member of the pearceite–polybasite group

Luca Bindi[1]*, Frank N. Keutsch[2], Dan Topa[3], Uwe Kolitsch[3,4], Marta Morana[1] and Kimberly T. Tait[5]

[1]Dipartimento di Scienze della Terra, Università degli Studi di Firenze, Via G. La Pira 4, I-50121 Firenze, Italy; [2]Paulson School of Engineering and Applied Sciences and Department of Chemistry and Chemical Biology, Harvard University, 12 Oxford Street, Cambridge, MA, USA.; [3]Department of Mineralogy and Petrography, Natural History Museum, Burgring 7, A-1010 Vienna, Austria; [4]Institute of Mineralogy and Crystallography, University of Vienna, Josef-Holaubek-Platz 2, A-1090 Vienna, Austria; and [5]Department of Natural History, Royal Ontario Museum, 100 Queens Park, Toronto, Ontario, Canada

Abstract

The chemistry and the crystal structure of the recently described mineral argentopolybasite are critically discussed based on the study of two new occurrences of the mineral: Gowganda, Timiskaming District, Ontario, Canada and IXL Mine, Silver Mountain mining district, Alpine County, California.

The crystal structure of argentopolybasite can be described as the sequence, along the **c** axis, of two alternating layers: a $[Ag_6Sb_2S_7]^{2-}$ *A* layer and a $[Ag_{10}S_4]^{2+}$ *B* layer. In the *B* layer there are linearly-coordinated metal positions (*B* sites), which are usually occupied by copper in all members of the pearceite–polybasite group, resulting in a *B*-layer composition $[Ag_9CuS_4]^{2+}$. In argentopolybasite, however, Ag fills all the metal sites in both *A* and *B* layers. By means of a multi-regression analysis on 67 samples of the pearceite–polybasite group, which were studied by electron microprobe and single-crystal X-ray diffraction, the effect of Ag, Sb and Se on the *B* sites of the *B* layer was modelled. Although the nomenclature rules for these minerals are based on chemical data only, we think this approach is useful to evaluate the goodness of the refinement of the structure (Ag/Cu disorder) and thus fundamental to discriminate different members of the pearceite–polybasite group.

Keywords: argentopolybasite, copper, pearceite–polybasite, structure refinement, electron probe micro-analysis

(Received 11 March 2023; accepted 13 April 2023; Accepted Manuscript published online: 2 May 2023; Associate Editor: František Laufek)

Introduction

The minerals of the pearceite–polybasite group, general formula $[M_6T_2X_7][M_{10}X_4]$ with M = Ag and Cu, T = As and Sb, and X = S, Se and Te, are fairly common in Nature. Eight members are known at present: argentopearceite (Sejkora *et al.*, 2020), argentopolybasite (Števko *et al.*, 2023), benleonardite (Bindi *et al.*, 2015), cupropearceite (Bindi *et al.*, 2007a, 2007c), cupropolybasite (Bindi *et al.*, 2007a, 2007c), pearceite (Bindi *et al.*, 2007a), polybasite (Bindi *et al.*, 2007a), and selenopolybasite (Bindi *et al.*, 2007a, 2007b).

Their crystal structure can be described as a sequence, along the **c** axis, of two alternating layers: a $[M_6T_2X_7]^{2-}$ *A* layer and a $[M_{10}X_4]^{2+}$ *B* layer (Bindi *et al.*, 2007a and references therein). As documented by Bindi *et al.* (2007a), these minerals can exhibit three different polytypes: the high-temperature fast-ion conductivity form (*Tac* polytype), the partially ordered form (*T2ac* polytype), and the low-temperature fully ordered form (*M2a2b2c* polytype).

Corresponding author: Luca Bindi; Email: luca.bindi@unifi.it
Cite this article: Bindi L., Keutsch F.N., Topa D., Kolitsch U., Morana M. and Tait K.T. (2023) First occurrence of the *M2a2b2c* polytype of argentopolybasite, $[Ag_6Sb_2S_7][Ag_{10}S_4]$: Structural adjustments in the Cu-free member of the pearceite–polybasite group. *Mineralogical Magazine* **87**, 561–567. https://doi.org/10.1180/mgm.2023.30

During an ongoing structural study of complex Ag (Cu)-bearing minerals in mineralogical collections from various museums, we found specimens containing Cu-free 'polybasite' (Bindi *et al.*, 2007a) from two different localities in North America. The same mineral has been recently approved by the International Mineralogical Association (IMA) as a new species with the name argentopolybasite (*T2ac* polytype) and the simplified formula $Ag_{16}Sb_2S_{11}$ (corresponding to the structural formula $[Ag_6Sb_2S_7][Ag_9AgS_4]$; Števko *et al.*, 2023). Interestingly, the As-dominant silver end-member argentopearceite ($Ag_{16}As_2S_{11}$; *T2ac* polytype), has also been recently discovered and described from the Lehnschafter mine, Czech Republic (Sejkora *et al.*, 2020). Those discoveries, in particular that related to argentopearceite, were surprising as it seemed that copper in the *B* layer was mandatory to stabilise these phases, especially when occurring in their disordered or partially ordered polytypes (Bindi *et al.*, 2006a, 2006b; 2013).

Given the presence of ubiquitous twinning, mobile Ag^+ and Cu^+ cations, satellite reflections due to commensurately modulated structures (giving rise to different polytypes) or to composite modulated structures, partially occupied sites and strong pseudo-symmetries, it is mandatory to critically evaluate the structural models obtained. The existence of two Cu- and

Se-free polybasite samples with excellent diffraction quality gives us the opportunity to critically elucidate this unusual crystal structure and the effect of Ag, Sb and Se on the *B* sites of the *B* layer.

Occurrence and chemical composition

The museum specimen (Fig. 1) used in the current work (Royal Ontario Museum, Canada; catalogue number M27183) is from Gowganda, Timiskaming District, Ontario, Canada, a well-established source of silver minerals. The geology of the deposit was studied and described by Andrews *et al.* (1986). Argentopolybasite occurs as black anhedral grains, up to 60 μm in length, with a black streak, associated closely with polybasite, calcite and chalcopyrite. An Ag-rich variety of polybasite from the same museum specimen was studied by Bindi and Menchetti (2009), who did not realise the presence of argento-polybasite at that time. Argentopolybasite and polybasite show no macroscopic/microscopic differences.

A second specimen containing argentopolybasite (Fig. 2) was collected independently at the IXL mine, Silver Mountain mining district, Alpine County, California (Clark and Evans, 1977), by Kyle Beucke and given for study to one of the authors (FNK). Associated minerals in the specimen include pyrite, argento-pearceite and acanthite. Both argentopolybasite and argento-pearceite occur as black anhedral grains in a quartz gangue.

The chemical composition of argentopolybasite from both occurrences was determined using wavelength-dispersive analysis (WDS) by means of a JEOL JXA-8200 (University of Florence, Italy) and a JEOL JXA-8530F (Natural History Museum of Vienna, Austria) electron probe micro-analyser. Major and minor elements were determined at a 25 kV accelerating voltage and a 20 nA beam current, with a spot size of 2 μm (no surface damage was observed when using these conditions). For the WDS analyses of the argentopolybasite from Gowganda the following lines were used: S*K*α, Fe*K*α, Cu*K*α, Zn*K*α, As*L*α, Se*L*α, Ag*L*α, Sb*L*β, Te*L*α, Au*M*α and Pb*M*α. For the WDS analyses of the argentopolybasite from the IXL mine the following lines were used: S*K*α, Cu*K*α, As*L*α, Se*K*α, Ag*L*α, Sb*L*α and Pb*M*α. The standards employed for Gowganda were: native elements for Cu, Ag, Au and Te; galena for Pb; pyrite for Fe and S; synthetic Sb_2S_3 for Sb; synthetic As_2S_3 for As; synthetic ZnS for Zn; and synthetic $PtSe_2$ for Se. The standards employed for the IXL mine were: lorándite for As; galena for Pb; chalcopyrite for Cu and S; native silver for Ag; stibnite for Sb; and synthetic Cu_2Se for Se. The detection limit for minor elements was 0.01 wt.%.

Figure 1. Argentopolybasite-*M*2*a*2*b*2*c*-bearing specimen (1.5 × 0.5 × 0.5 cm) from Gowganda, Timiskaming District, Ontario (Canada), ROM accession number M27183; the specimen also contains polybasite, calcite and chalcopyrite. Courtesy of ROM (Royal Ontario Museum), Toronto, Canada. ©ROM. Photograph by Tina Weltz.

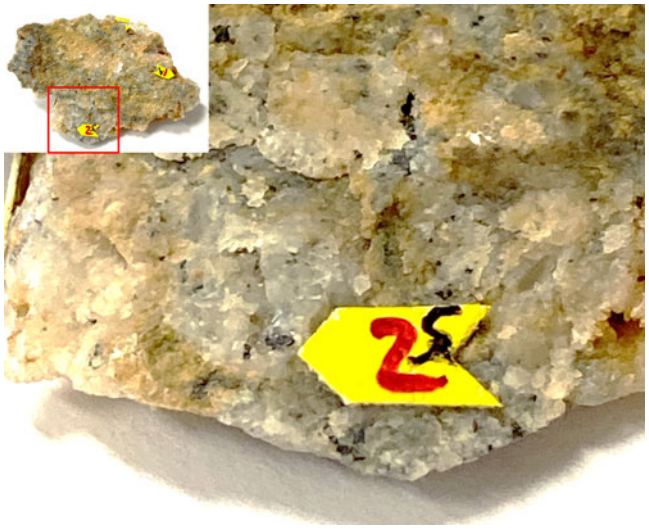

Figure 2. Argentopolybasite-*T*2*ac*-bearing specimen (6 cm wide) from the IXL mine, Silver Mountain mining district, Alpine County, California. The specimen also contains pyrite, argentopearceite and acanthite.

The argentopolybasite fragments from both specimens were found to be homogeneous within analytical error. The average chemical compositions ($N = 5$ and 4 for argentopolybasite from Gowganda and IXL mine, respectively) are reported in Table 1. On the basis of 29 atoms, the formula can be written as $(Ag_{16.00}Cu_{0.02})_{\Sigma 16.02}(Sb_{1.95}As_{0.04})_{\Sigma 1.99}S_{10.99}$ and $(Ag_{16.04}Cu_{0.02}Pb_{0.01})_{\Sigma 16.07}(Sb_{1.37}As_{0.56})_{\Sigma 1.93}(S_{10.46}Se_{0.54})_{\Sigma 11.00}$, for argentopolybasite from Gowganda and IXL mine, respectively.

X-ray crystallography

Unit-cell parameters for argentopolybasite from Gowganda are: $a = 26.384(2)$, $b = 15.232(1)$, $c = 24.148(2)$ Å, $\beta = 90.03(1)°$ and $V = 9704.6(1)$ Å^3, indicating the *M*2*a*2*b*2*c* polytype (Bindi *et al.*, 2007a). On the contrary, hexagonal unit-cell parameters for argentopolybasite from IXL mine are: $a = 15.061(2)$, $c = 12.308(2)$ Å and $V = 2417.8(2)$ Å^3, indicating the *T*2*ac* polytype (Bindi *et al.*, 2007a). Given the much better diffraction quality and the

Table 1. Mean analytical data (in wt.%) for argentopolybasite.

Constituent	Gowganda	IXL Mine
Ag	74.32	74.24
Cu	0.05	0.06
Pb	0.02	0.08
Zn	0.01	n.a.
Fe	0.01	b.d.l.
Au	0.02	n.a.
Sb	10.17	7.16
As	0.13	1.79
S	15.08	14.38
Se	0.01	1.83
Te	0.02	n.a.
Total	99.43	99.54

Note: n.a. = not analysed; b.d.l. = below detection limit

https://doi.org/10.1180/mgm.2023.30 Published online by Cambridge University Press

fact that the trigonal polytype was already reported by Števko *et al.* (2023), we present here only the structural data for argentopolybasite-*M*2*a*2*b*2*c* from Gowganda.

A small argentopolybasite fragment (0.055 × 0.040 × 0.032 mm in size) was extracted from the M27183 sample and mounted on a 5 μm diameter carbon fibre, which was, in turn, attached to a glass rod. As pearceite–polybasite minerals are usually twinned (Bindi *et al.*, 2020 and references therein), a full diffraction sphere was collected at ambient temperature using an Oxford Diffraction Xcalibur 3 single-crystal diffractometer. Refined unit-cell parameters are: $a = 26.384(2)$, $b = 15.232(1)$, $c = 24.148(2)$ Å, $\beta = 90.03(1)°$ and $V = 9704.6(1)$ Å^3 ($Z = 16$). Intensity integration and standard Lorentz-polarisation corrections were done with the *CrysAlis RED* (Oxford Diffraction, 2006) software package. The program *ABSPACK* of the *CrysAlis RED* package was used for the multi-scan absorption correction. Subsequent calculations were conducted with the *JANA2006* program suite (Petříček *et al.*, 2006). The refinement of the structure was carried out in the space group *C*2/*c* starting from the atomic coordinates given by Bindi and Menchetti (2009) for the crystal structure of Ag-rich polybasite-*M*2*a*2*b*2*c*. Site-scattering values were refined using scattering curves (Wilson, 1992) for neutral species for the Sb sites (Sb *vs* As) and for the Cu sites (Ag *vs* Cu) of the *B* layer (hereafter labelled *B* sites). The Sb sites and the *B* sites were found to be fully occupied by antimony and silver, respectively, and their occupancies were fixed during subsequent refinement cycles. With the introduction of twinning by metric merohedry (see Evain *et al.*, 2006) the refinement smoothly converged to $R = 0.103$ for observed reflections [2σ(*I*) level], including all the collected reflections in the refinement. Indeed, the peculiar geometry of the pseudo-orthorhombic unit cell (with $a \approx 3^{½} \cdot b$) makes a {110} twinning very probable. Based on this refinement, the analyses of the difference-Fourier synthesis

Table 2. Crystallographic data for the selected argentopolybasite-*M*2*a*2*b*2*c* crystal.

Crystal data	
Mineral	Argentopolybasite
Chemical formula	$Ag_{16}Sb_2S_{11}$
Temperature (K)	298(2)
Space group	*C*2/*c*
Cell parameters:	
a (Å)	26.384(2)
b (Å)	15.232(1)
c (Å)	24.148(2)
β (°)	90.03(1)
V (Å^3)	9704.6(1)
Z	16
Data collection	
Crystal colour	black
Crystal shape	block
Crytal size (mm)	0.032 × 0.040 × 0.055
Diffractometer	Oxford Diffraction Xcalibur 3
Radiation	Mo*K*α
$\sin\theta/\lambda_{max}$ (Å^{-1}) / θ_{max} (°)	0.801 / 34.72
Coverage (%) at θ_{max}	99
hkl range	$-41 \le h \le 41$ $-23 \le k \le 23$ $-38 \le l \le 38$
Data refinement	
No. of independent reflections	18,461
Criterion for obs.	$I > 2\sigma(I)$
No. of observed refl.	11,867
R_{int}	0.0412
Refined parameters	443
Polychromatic point group for first-degree twin	$K_{WB}^{(3)} = \left(\bar{3}^{(3)}\ \frac{2^{(2,1)}}{m^{(2,1)}}\right)^{(3)}$
Twin matrices	$\begin{bmatrix} 1 & 0 & 0 \\ 0 & 1 & 0 \\ 0 & 0 & 1 \end{bmatrix}, \begin{bmatrix} -1/2 & 1/2 & 0 \\ -3/2 & -1/2 & 0 \\ 0 & 0 & 1 \end{bmatrix}, \begin{bmatrix} -1/2 & -1/2 & 0 \\ 3/2 & -1/2 & 0 \\ 0 & 0 & 1 \end{bmatrix}$

Table 3. Atoms, fractional atomic coordinates and equivalent isotropic displacement parameters (Å^2) for the selected argentopolybasite-*M*2*a*2*b*2*c* crystal from Gowganda.

Atom	*x*	*y*	*z*	U_{eq}
Sb1	0.16691(2)	0.24568(4)	0.04551(3)	0.02390(13)
Sb2	0.16614(2)	0.75682(4)	0.04760(3)	0.02314(12)
Sb3	0.42097(3)	−0.00615(4)	0.04548(3)	0.02750(14)
Sb4	0.41115(3)	0.50121(4)	0.04669(3)	0.02540(13)
Ag1	0.03321(3)	0.14641(5)	0.05461(3)	0.02381(14)
Ag2	0.04441(3)	0.36053(5)	0.06740(3)	0.02963(16)
Ag3	0.04226(3)	0.63239(5)	0.06980(3)	0.03086(16)
Ag4	0.03024(3)	0.86014(6)	0.05619(4)	0.03431(17)
Ag5	0.16431(3)	0.00340(4)	0.07375(3)	0.02338(14)
Ag6	0.18510(3)	0.50140(4)	0.05036(3)	0.02526(15)
Ag7	0.28764(3)	0.10215(5)	0.05251(3)	0.02563(14)
Ag8	0.28426(3)	0.37816(5)	0.06410(3)	0.02702(15)
Ag9	0.28844(3)	0.62838(5)	0.06431(3)	0.02505(14)
Ag10	0.28740(3)	0.89928(5)	0.05731(3)	0.02605(14)
Ag11	0.43054(3)	0.25110(5)	0.05747(4)	0.02999(16)
Ag12	0.41695(3)	0.74575(4)	0.06320(3)	0.02297(14)
Ag13	0.16010(3)	0.00619(4)	0.19916(3)	0.02222(14)
Ag14	0.34440(3)	0.03098(4)	0.18214(3)	0.02314(14)
Ag15	0.46083(3)	0.01073(4)	0.19471(3)	0.02405(14)
Ag16	0.09771(3)	0.19267(5)	0.19881(3)	0.02802(15)
Ag17	0.22637(3)	0.17237(5)	0.19512(3)	0.02740(15)
Ag18	0.41216(3)	0.20899(5)	0.18777(3)	0.02554(14)
Ag19	0.05187(2)	0.37819(4)	0.19633(3)	0.02187(13)
Ag20	0.17394(2)	0.37676(4)	0.19206(3)	0.02311(13)
Ag21	0.29034(3)	0.36017(4)	0.19443(3)	0.02379(14)
Ag22	0.40171(3)	0.41655(4)	0.19273(3)	0.02481(14)
Ag23	0.06024(3)	0.63446(5)	0.19426(3)	0.02585(14)
Ag24	0.18806(3)	0.62956(5)	0.18622(3)	0.02689(15)
Ag25	0.31385(3)	0.60678(5)	0.19050(3)	0.02585(14)
Ag26	0.46801(2)	0.59315(4)	0.18471(3)	0.02055(13)
Ag27	0.02232(2)	0.90310(4)	0.18660(3)	0.02034(13)
Ag28	0.13268(3)	0.80878(5)	0.19468(3)	0.02781(15)
Ag29	0.26177(3)	0.84456(5)	0.19285(3)	0.02928(16)
Ag30	0.41352(3)	0.80102(5)	0.18812(3)	0.02606(14)
B1 (Ag)	0	0.24475(11)	¼	0.0256(3)
B2 (Ag)	0	0.74655(11)	¼	0.0298(4)
B3 (Ag)	0.24338(5)	0.50483(8)	0.24935(6)	0.0311(3)
S1	0.11902(11)	0.14149(18)	0.09743(12)	0.0348(6)
S2	0.13475(11)	0.37550(18)	0.09219(12)	0.0344(6)
S3	0.24675(12)	0.2345(2)	0.09678(14)	0.0403(6)
S4	0.13464(10)	0.62891(17)	0.09323(11)	0.0297(5)
S5	0.11974(10)	0.86334(18)	0.10389(12)	0.0323(5)
S6	0.24578(11)	0.75742(18)	0.09717(13)	0.0350(6)
S7	0.49696(11)	−0.00545(17)	0.10375(13)	0.0340(6)
S8	0.37820(10)	0.11673(18)	0.08883(12)	0.0343(6)
S9	0.37899(10)	0.37537(19)	0.09527(13)	0.0356(6)
S10	0.49500(13)	0.50201(18)	0.08751(15)	0.0383(7)
S11	0.37774(10)	0.6146(2)	0.10800(13)	0.0370(6)
S12	0.37495(10)	0.88612(18)	0.09878(12)	0.0316(5)
S13	0.22948(11)	−0.00524(16)	−0.00027(13)	0.0339(6)
S14	0.49126(10)	0.77315(19)	0.00101(11)	0.0334(5)
S15	0.07471(12)	0.0171(2)	0.23208(14)	0.0402(6)
S16	0.24825(12)	0.00408(18)	0.15216(15)	0.0399(7)
S17	0.01688(10)	0.25707(17)	0.15271(12)	0.0295(5)
S18	0.32914(11)	0.22636(18)	0.23173(12)	0.0344(5)
S19	0.10120(11)	0.50514(17)	0.23299(14)	0.0357(6)
S20	0.24730(12)	0.49353(17)	0.15005(14)	0.0364(6)
S21	0.01109(12)	0.74163(19)	0.15147(14)	0.0391(6)
S22	0.33200(13)	0.7524(2)	0.23559(15)	0.0417(7)

https://doi.org/10.1180/mgm.2023.30 Published online by Cambridge University Press

maps suggested an additional twin law with a twofold axis, perpendicular to the previous threefold axis as a generator twin element, thus leading to a second-degree twin. The introduction of only three new parameters (the new twin volume ratios) dramatically lowered the *R* value to 0.055, although the new domains were rather small [volume percentages: 4.12(4)%, 3.05(2)% and 2.54(3)%].

A non-harmonic approach with a Gram–Charlier development of the Debye–Waller factors up to the third order (Johnson and Levy, 1974; Kuhs, 1984; Bindi and Evain, 2007) was then used to describe the electron density in the vicinity of four Ag atoms (i.e. Ag15, Ag22, Ag24 and Ag29) for which residues were found in the difference-Fourier maps. Using this approach, with anisotropic atomic displacement parameters for all the atoms and no constraints, the residual value settled at $R = 0.0334$ ($Rw = 0.0915$) for 11,867 independent observed reflections [$2\sigma(I)$ level] and 443 parameters, and at $R = 0.0380$ ($Rw = 0.0945$) for all 18,461 independent reflections. Experimental details are given in Table 2. Atomic coordinates and bond distances are reported in Table 3 and 4, respectively. The crystallographic information file has been deposited with the Principal Editor of *Mineralogical Magazine* and is available as Supplementary material (see below).

Results and discussion

As illustrated in previous structural studies (Bindi *et al.*, 2020 and references therein), the crystal structure of the monoclinic polytype (*M*2*a*2*b*2*c*) of argentopolybasite (Fig. 3) can be described as the sequence, along the **c** axis, of two alternating layers: a $[M_6T_2X_7]^{2-}$ *A* (or *A*') layer and a $[M_{10}X_4]^{2+}$ *B* (or *B*') layer (*A*,*B* and *A*',*B*' being related by a *c* glide reflection).

In the $[M_6T_2X_7]^{2-}$ *A* (or *A*') layer, each silver cation is threefold coordinated by sulfur. The Sb atoms are the top of a trigonal pyramid with the three S atoms forming a base. In the $[M_{10}X_4]^{2+}$ *B* (or *B*') layer, the 18 independent Ag atoms show different environments from quasi-linear to quasi-tetrahedral (Table 4). Argentopolybasite shows the presence of Ag at all the B structural positions of the *B* layer. The B positions [B1, B2 (4*e*) and B3 (8*f*)] are generally occupied by copper in pearceite–polybasite minerals in a nearly perfect linear coordination (see Bindi *et al.*, 2020 and references therein). In argentopolybasite, the mean Ag–S bond distances at the B sites, i.e. 2.399, 2.398 and 2.397 Å, for B1, B2 and B3, respectively, are very close to those observed for the linearly-coordinated Ag atoms of the *B* layer (Table 4) and exhibit bond-valence sums close to 1.00 (0.94–0.95 valence units, Brese and O'Keeffe, 1991). In the trigonal *T*2*ac* polytype of argentopolybasite (Števko *et al.*, 2023) the two *B* sites (labelled Ag11 and Cu12) show mean bond distances of 2.244 and 2.230 Å in the refined structure model of these authors ($R = 0.0741$; four-fold twinning was modelled). The two sites also show partial occupancy: Ag11 = 0.687(10)Ag and Cu12 = 0.82(3)Cu. This is bizarre because the *B* sites always act as a fully-occupied, ordered part surrounded by mobile cations in the *B* layer (Bindi *et al.*, 2006a, 2020). Furthermore, the occupancy of the *B* sites is strictly correlated with the way the mobile part (liquid-like structure) has been modelled and the approach considered to deal with the pervasive twinning.

To try to elucidate this discrepancy, we carried out a multi-regression analysis on 67 samples of the pearceite–polybasite group which were studied by both electron probe micro-analyser and single-crystal X-ray diffraction (Bindi *et al.*, 2020, references therein and unpublished data). The analysis allows modelling of

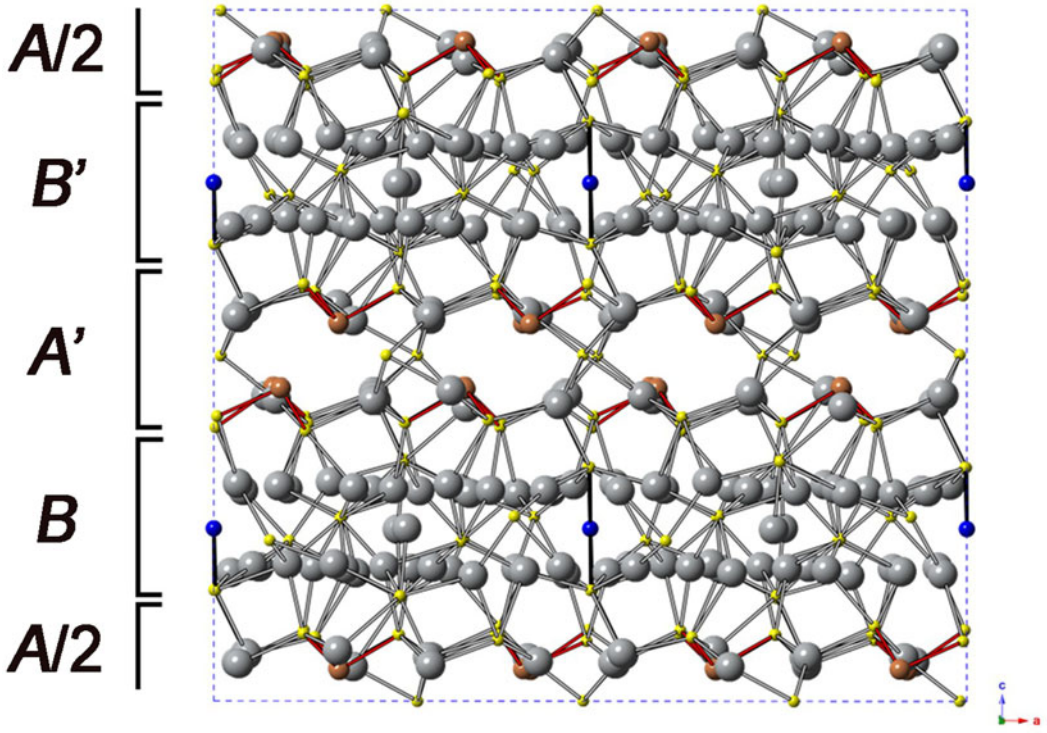

Figure 3. Projection of the argentopolybasite-*M*2*a*2*b*2*c* structure along the monoclinic *b* axis, emphasising the succession of the $[M_6T_2X_7]^{2-}$ *A* (or *A*') and $[M_{10}X_4]^{2+}$ *B* (*B*') layers. Grey, orange and yellow spheres indicate Ag, Sb and S atoms, respectively. Blue spheres indicate the linearly-coordinated *B* positions. The unit cell is outlined. *A*,*B* and *A*',*B*' are related by a *c* glide reflection. Drawn using *VESTA* (Momma and Izumi, 2011).

https://doi.org/10.1180/mgm.2023.30 Published online by Cambridge University Press

Table 4. Main interatomic distances (Å) for the selected argentopolybasite-*M2a2b2c* crystal from Gowganda.

Sb1–S1	2.385(3)	Ag5–S13	2.484(3)	Ag13–S15	2.395(3)	Ag21–S18	2.452(3)	Ag29–S22	2.543(3)
Sb1–S2	2.429(3)	Ag5–S1	2.486(3)	Ag13–S16	2.589(3)	Ag21–S20	2.562(3)	Ag29–S16	2.645(3)
Sb1–S3	2.449(3)	Ag5–S5	2.543(3)	Ag13–*B*3	2.8334(16)	Ag21–*B*3	2.8551(15)	Ag29–S6	2.698(3)
		Ag5–S16	2.913(4)					Ag29–*B*3	2.8155(15)
Sb2–S4	2.388(3)			Ag14–S19	2.532(3)	Ag22–S15	2.455(3)		
Sb2–S6	2.418(3)	Ag6–S2	2.542(3)	Ag14–S16	2.669(3)	Ag22–S9	2.508(3)	Ag30–S22	2.548(3)
Sb2–S5	2.445(3)	Ag6–S13	2.559(3)	Ag14–S8	2.753(3)			Ag30–S12	2.715(3)
		Ag6–S4	2.572(3)	Ag14–*B*3	2.8747(16)	Ag23–S21	2.327(3)	Ag30–*B*1	2.8583(9)
Sb3–S12	2.413(3)	Ag6–S20	2.915(3)			Ag23–S19	2.433(3)	Ag30–S17	2.936(3)
Sb3–S8	2.424(3)			Ag15–S19	2.395(3)	Ag23–B2	2.6935(13)		
Sb3–S7	2.449(3)	Ag7–S3	2.525(3)	Ag15–S7	2.408(3)			B1–S17 (×2)	2.399(3)
		Ag7–S8	2.554(3)	Ag16–S17	2.597(3)	Ag24–S18	2.511(3)	B1–Ag19	2.7723(14)
Sb4–S9	2.402(3)	Ag7–S13	2.579(3)	Ag16–S22	2.603(4)	Ag24–S4	2.651(3)	B1–Ag30 (×2)	2.8583(9)
Sb4–S10	2.421(3)			Ag16–S1	2.630(3)	Ag24–S20	2.739(3)	B1–Ag26 (×2)	2.9205(14)
Sb4–S11	2.440(3)	Ag8–S13	2.501(3)	Ag16–S15	2.858(3)	Ag24–*B*3	2.8392(16)	B1–Ag16	2.9676(9)
		Ag8–S3	2.528(3)						
Ag1–S1	2.490 (3)	Ag8–S9	2.610(3)	Ag17–S22	2.581(3)	Ag25–S22	2.517(3)	B2–S21 (×2)	2.398(3)
Ag1–S10	2.547 (3)	Ag8–S20	2.890(3)	Ag17–S3	2.613(3)	Ag25–S11	2.613(3)	B2–Ag23	2.6935(13)
Ag1–S14	2.574 (3)			Ag17–S16	2.825(3)	Ag25–S20	2.648(3)	B2–Ag18 (×2)	2.8201(9)
Ag1–S17	2.939 (3)	Ag9–S6	2.400(3)	Ag17–S18	2.968(3)	Ag25–*B*3	2.8090(15)	B2–Ag27	2.8944(16)
		Ag9–S13	2.476(3)						
Ag2–S2	2.468(3)	Ag9–S11	2.590(3)	Ag18–S18	2.449(3)	Ag26–S15	2.579(3)	B3–S16	2.388(4)
Ag2–S14	2.511(3)			Ag18–S21	2.798(3)	Ag26–S10	2.819(3)	B3–S20	2.406(4)
Ag2–S7	2.551(3)	Ag10–S12	2.525(3)	Ag18–*B*2	2.8201(9)	Ag26–S17	2.914(3)	B3–Ag29	2.8155(15)
Ag2–S17	2.694(3)	Ag10–S13	2.526(3)	Ag18–S8	2.913(3)	Ag26–*B*1	2.9205(15)	B3–Ag13	2.8334(16)
		Ag10–S6	2.608(3)					B3–Ag14	2.8747(16)
Ag3–S14	2.403(3)			Ag19–S17	2.316(3)	Ag27–S15	2.476(3)	B3–Ag17	2.9910(15)
Ag3–S4	2.503(3)	Ag11–S9	2.503(3)	Ag19–S19	2.493(3)	Ag27–S21	2.618(3)		
Ag3–S7	2.552(3)	Ag11–S14	2.528(3)	Ag19–*B*1	2.7723(14)	Ag27–*B*2	2.8944(16)		
Ag3–S21	2.709(3)	Ag11–S8	2.583(3)			Ag27–S10	2.918(3)		
				Ag20–S22	2.582(3)				
Ag4–S10	2.471(3)	Ag12–S11	2.496(3)	Ag20–S2	2.623(3)	Ag28–S5	2.369(3)		
Ag4–S14	2.520(3)	Ag12–S14	2.505(3)	Ag20–S20	2.818(3)	Ag28–S18	2.397(3)		
Ag4–S5	2.627(3)	Ag12–S12	2.557(3)	Ag20–S19	2.913(3)				
Ag4–S21	2.968(3)								

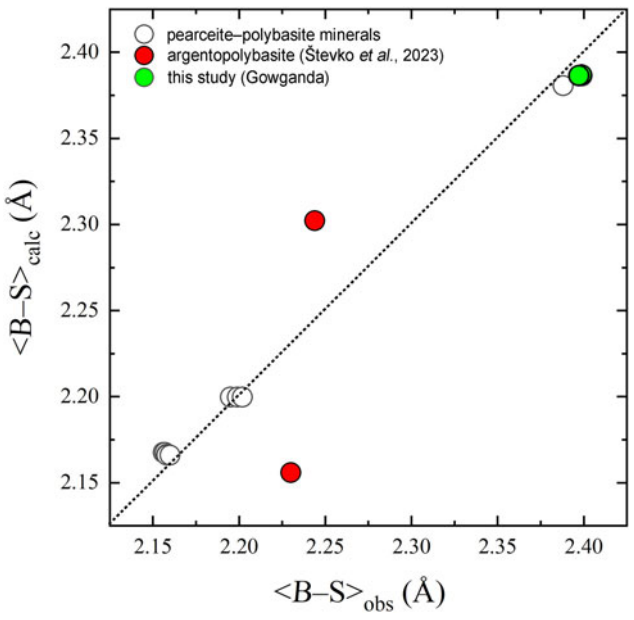

Figure 4. Multi-regression analysis (see text) showing the combined effect of Ag, Sb and Se on the linearly-coordinated *B*–S distance of the *B* layer. Red circles refer to the *B*–S distances in holotype argentopolybasite-*T2ac* studied by Števko *et al.* (2023). Green circles refer to the *B*–S distances in argentopolybasite of the current study (Gowganda). Standard uncertainties are smaller than the size of the symbols.

the *B*–S distance of the linearly-coordinated Ag atom in the *B* layer on the basis of the Ag, Sb and Se contents, i.e. *B*–S (Å) = 2.101(8) + 0.213(5)Ag atoms per formula unit (apfu) + 0.037(5)Sb apfu + 0.012(2)Se apfu. The observed (derived from structure refinements) versus calculated (with the equation above) bond distances are shown in Fig. 4. Although there is not a large variation of the distribution of the *B*–S distances mainly due to the rarity of Cu-free members, the two values obtained by Števko *et al.* (2023) for holotype argentopolybasite-*T2ac* are clearly off the main trend. This could imply either that the crystal they used for the structural study is not that analysed by electron microprobe or that the site occupancy and/or twinning was not modelled properly. To corroborate the hypothesis of a likely problem with the structure refinement there is the fact that the unit-cell and the overall geometry of the mineral studied by Števko *et al.* (2023) perfectly fit the trend expected for Cu-free polybasite and argentopolybasite *sensu stricto*. In the structure of these minerals, disregarding the polytype, the *B*–S bond distances are mainly lined along the **c** axis (Fig. 3). This means that when Ag substitutes for Cu in these structural positions an increase in the *c* parameter and a consequent increase in the volume of the unit cell are expected. This is easily observable by plotting the unit-cell volume as a function of the copper content obtained by electron microprobe. To compare all the members belonging to the pearceite–polybasite group, the variation of the hexagonal subcell volume (i.e. $a \approx 7.5$ and $c \approx 12$ Å) was considered. Argentopolybasite of the present investigation and that

https://doi.org/10.1180/mgm.2023.30 Published online by Cambridge University Press

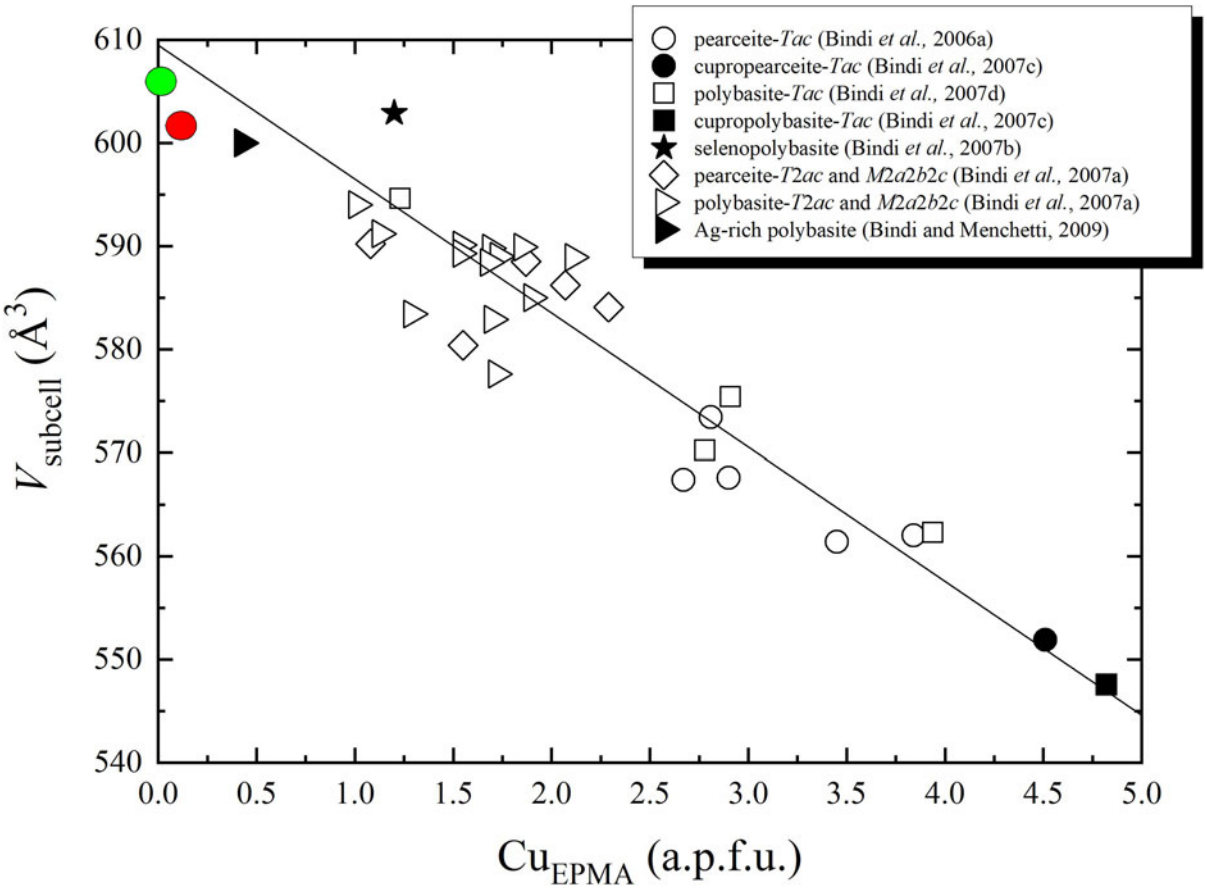

Figure 5. Relationship between the unit-cell volume of the hexagonal subcell (Å^3) and the copper content obtained by electron probe micro-analysis [Cu_{EPMA}] (apfu) for the different members of the pearceite–polybasite group (from Bindi *et al*., 2006a, 2007a,b,c,d; Bindi and Menchetti, 2009). Green and red circles indicate argentopolybasite of the current study (Gowganda) and that studied by Števko *et al.* (2023), respectively. Standard uncertainties are smaller than the size of the symbols.

studied by Števko *et al.* (2023) (green and red circles in Fig. 5) are an excellent fit for the general trend observed for the minerals of the pearceite–polybasite group.

The discovery of argentopolybasite and argentopearceite demonstrates that there could be other surprises hidden in this complex group of minerals. It is critical to further study them for the advancement of the knowledge about processes relevant for Earth and to share that knowledge with others such as in environmental and material sciences.

Acknowledgements. We thank Federica Zaccarini, one anonymous reviewer, Pete Leverett, and the Associate Editor Frantisek Laufek for their constructive comments. LB wishes to thank MIUR-PRIN2017, project "TEOREM deciphering geological processes using Terrestrial and Extraterrestrial ORE Minerals", protocol 2017AK8C32. FNK thanks the Harvard University Center for Nanoscale Systems (CNS), which is supported by the National Science Foundation under NSF award no. ECCS-2025158.

Supplementary material. The supplementary material for this article can be found at https://doi.org/10.1180/mgm.2023.30.

Competing interests. The authors declare none.

References

Andrews A.J., Owsiacki L., Kerrich R. and Strong D.F. (1986) The silver deposits at Cobalt and Gowganda, Ontario. I. Geology, petrography and whole-rock geochemistry. *Canadian Journal of Earth Sciences*, **23**, 1480–1506.

Bindi L. and Evain M. (2007) Gram-Charlier development of the atomic displacement factors into mineral structures: The case of samsonite, $Ag_4MnSb_2S_6$. *American Mineralogist*, **92**, 886–891.

Bindi L. and Menchetti S. (2009) Adding further complexity to the polybasite structure: The role of silver in the *B* layer of the *M2a2b2c* polytype. *American Mineralogist*, **94**, 151–155.

Bindi L., Evain M. and Menchetti S. (2006a) Temperature dependence of the silver distribution in the crystal structure of natural pearceite, $(Ag,Cu)_{16}(As,Sb)_2S_{11}$. *Acta Crystallographica*, **B62**, 212–219.

Bindi L., Evain M., Pradel A., Albert S., Ribes M. and Menchetti S. (2006b) Fast ionic conduction character and ionic phase-transitions in disordered crystals: The complex case of the minerals of the pearceite-polybasite group. *Physics and Chemistry of Minerals*, **33**, 677–690.

Bindi L., Evain M., Spry P.G. and Menchetti S. (2007a) The pearceite-polybasite group of minerals: Crystal chemistry and new nomenclature rules. *American Mineralogist*, **92**, 918–925.

Bindi L., Evain M. and Menchetti S. (2007b) Selenopolybasite, $[(Ag,Cu)_6(Sb,As)_2(S,Se)_7][Ag_9Cu(S,Se)_2Se_2]$, a new member of the pearceite-polybasite group from the De Lamar Mine, Owyhee county, Idaho, USA. *The Canadian Mineralogist*, **45**, 1525–1528.

Bindi L., Evain M., Spry P.G., Tait K.T. and Menchetti S. (2007c) Structural role of copper in the minerals of the pearceite-polybasite group: The case of the new minerals cupropearceite and cupropolybasite. *Mineralogical Magazine*, **71**, 641–650.

Bindi L., Evain M. and Menchetti S. (2007d) Complex twinning, polytypism and disorder phenomena in the crystal structures of antimonpearceite and arsenpolybasite. *The Canadian Mineralogist*, **45**, 321–333.

Bindi L., Schaper A.K., Kurata H. and Menchetti S. (2013) The composite modulated structure of cupropearceite and cupropolybasite and its behavior toward low temperature. *American Mineralogist*, **98**, 1279–1284.

Bindi L., Stanley C. and Spry P.G. (2015) New structural data reveal benleonardite to be a member of the pearceite-polybasite group. *Mineralogical Magazine*, **79**, 1213–1221.

Bindi L., Nespolo M., Krivovichev S.V., Chapuis G. and Biagioni C. (2020) Producing highly complicated materials. Nature does it better. *Reports on Progress in Physics*, **83**, 106501.

Brese N.E. and O'Keeffe M. (1991) Bond-valence parameters for solids. *Acta Crystallographica*, **B47**, 192–197.

Clark W.B. and Evans J.R. (1977) Mines and mineral resources of Alpine County, California. *California Division Mines and Geology County Report*, **8**, 28–29, 30, 45.

Evain M., Bindi L. and Menchetti S. (2006) Structural complexity in minerals: twinning, polytypism and disorder in the crystal structure of polybasite, $(Ag,Cu)_{16}(Sb,As)_2S_{11}$. *Acta Crystallographica*, **B62**, 447–456.

Johnson C.K. and Levy H.A. (1974) Thermal motion analysis using Bragg diffraction data. Pp. 311–336 in: *International Tables for X-ray Crystallography Vol. IV* (J.A. Ibers and W.C. Hamilton, editors). Kynoch Press, Birmingham, UK.

Kuhs W.F. (1984) Site-symmetry restrictions on thermal-motion-tensor coefficients up to rank 8. *Acta Crystallographica*, **A40**, 133–137.

Momma K. and Izumi F. (2011) VESTA 3 for three-dimensional visualization of crystal, volumetric and morphology data. *Journal of Applied Crystallography*, **44**, 1272–1276.

Oxford Diffraction (2006) *CrysAlis RED (Version 1.171.31.2) and ABSPACK in CrysAlis RED*. Oxford Diffraction Ltd, Abingdon, Oxfordshire, England.

Petříček V., Dušek M. and Palatinus L. (2006) *JANA2006, a crystallographic computing system*. Institute of Physics, Academy of Sciences of the Czech Republic, Prague, Czech Republic.

Sejkora J., Plášil J., Makovicky E., Škácha P., Dolníček Z. and Gramblička R. (2020) Argentopearceite, IMA 2020-049, in: CNMNC Newsletter 57. *Mineralogical Magazine*, **84**, 791–794, https://doi.org/10.1180/mgm.2020.73

Števko M., Mikuš T., Sejkora J., Plášil J., Makovicky E., Vlasáč J. and Kasatkin A. (2023) Argentopolybasite, $Ag_{16}Sb_2S_{11}$, a new member of the polybasite group. *Mineralogical Magazine*, 382–395, https://doi.org/10.1180/mgm.2022.141

Wilson A.J.C. (editor) (1992) *International Tables for Crystallography, Volume C: Mathematical, Physical and Chemical Tables*. Kluwer Academic, Dordrecht, The Netherlands.

https://doi.org/10.1180/mgm.2023.30 Published online by Cambridge University Press